ANZIAM J. 61(2019), 1–22
doi:10.1017/S1446181118000287

A RAYLEIGH–RITZ METHOD FOR NAVIER–STOKES FLOW THROUGH CURVED DUCTS

BRENDAN HARDING

(Received 24 May, 2018; accepted 10 October, 2018; first published online 11 January 2019)

Abstract

We present a Rayleigh–Ritz method for the approximation of fluid flow in a curved duct, including the secondary cross-flow, which is well known to develop for nonzero Dean numbers. Having a straightforward method to estimate the cross-flow for ducts with a variety of cross-sectional shapes is important for many applications. One particular example is in microfluidics where curved ducts with low aspect ratio are common, and there is an increasing interest in nonrectangular duct shapes for the purpose of size-based cell separation. We describe functionals which are minimized by the axial flow velocity and cross-flow stream function which solve an expansion of the Navier–Stokes model of the flow. A Rayleigh–Ritz method is then obtained by computing the coefficients of an appropriate polynomial basis, taking into account the duct shape, such that the corresponding functionals are stationary. Whilst the method itself is quite general, we describe an implementation for a particular family of duct shapes in which the top and bottom walls are described by a polynomial with respect to the lateral coordinate. Solutions for a rectangular duct and two nonstandard duct shapes are examined in detail. A comparison with solutions obtained using a finite-element method demonstrates the rate of convergence with respect to the size of the basis. An implementation for circular cross-sections is also described, and results are found to be consistent with previous studies.

2010 *Mathematics subject classification*: primary 65M60; secondary 76D05.

Keywords and phrases: Rayleigh–Ritz method, Navier–Stokes equations, curved microfluidic duct, Dean flow.

1. Introduction

This paper is motivated by a technical note in which Wang [16] describes a Rayleigh–Ritz method for Stokes flow in a curved duct. Wang's own motivation was the consideration of miniaturized fluid devices in which typical Reynolds numbers are of the order of 10^{-3} or lower, at which the magnitude of the secondary cross-flow, well known to develop in curved ducts since the work of Dean [3], is negligible.

[1]School of Mathematical Sciences, The University of Adelaide, South Australia 5005, Australia; e-mail: brendan.harding@adelaide.edu.au.

Whilst results were provided for rectangular and elliptical shaped ducts, the method is applicable to ducts having arbitrary cross-sectional shape (one need only construct a function g which is zero on the boundary and positive on the interior of the cross-section, and be able to accurately approximate the integral of functions defined over the cross-section). Wang describes the method as being versatile and superior to finite-element methods as: (a) the domain need not be discretized, (b) boundary conditions are embedded in the basis functions, and (c) the memory requirements are much less.

We too are interested in miniaturized fluid apparatus, and a motivation for this work is the use of curved ducts for the separation and sorting of particles/cells in microfluidic devices [5, 8, 14]. Whilst the duct dimensions in these applications are quite small, the flow rates are sufficiently high, in order to obtain reasonable throughput/flux, that the Reynolds number can be as high as $O(100)$ and the effects of the secondary cross-flow cannot be neglected. Indeed, the additional effect of the secondary flow on particles is generally assumed to contribute towards the enhanced separation that is observed in these devices. Furthermore, some experiments have found nonrectangular ducts to be superior in some applications. An example of this is spiral ducts having trapezoidal cross-section which have been reported as more efficient devices for size-based cell separation/isolation [18]. Studies of the inertial lift force rely on a separation of the fluid behaviour with and without a particle; a recent example which considered the effect of inertial migration within a straight square duct utilized a truncated Fourier expansion of the background flow [12]. Extending this methodology to curved ducts and nonrectangular shapes will similarly require an approximation of the fluid flow that is both simple and efficient to evaluate.

Whilst flow in curved ducts having circular and rectangular cross-sections has been studied extensively [6, 15, 19, 20], the methods employed are generally specific to circular or rectangular ducts and cannot be readily adapted to other shapes. Fluid flow through spiral ducts having cross-sections with small aspect ratio and variable top wall shape has also been explored [11]. In contrast, here we consider the curved duct to have a constant bend radius, allow for a larger range of duct shapes and not require separate corrections near the side walls.

In this paper, we extend Wang's approach to moderate Dean number (Dn) by developing a Rayleigh–Ritz method to approximate the secondary cross-flow in addition to the axial flow. We begin with the standard Navier–Stokes equations in a cylindrical coordinate system to model steady pressure-driven flow through a curved duct in Section 2. The equations are then nondimensionalized and the pressure is eliminated, leading to equations in terms of the axial flow component u and a stream function Φ describing the secondary flow within the cross-sectional plane. The approach is similar to that of Dean and Hurst [4] but using an alternative scaling and without eliminating any terms based on a small characteristic channel length relative to the bend radius. Upon applying a perturbation expansion to both u and Φ with respect to the square of the Dean number, we obtain a sequence of partial differential equations (PDEs) satisfied by successively higher-order corrections to the flow.

https://doi.org/10.1017/S1446181118000287 Published online by Cambridge University Press

A general form of the Rayleigh–Ritz method for approximating the flow is developed in Section 3.1. Since the equations for the leading-order axial flow component are exactly the Stokes model considered by Wang [16], the same Rayleigh–Ritz method can be applied. On the other hand, the leading-order Φ component is governed by an inhomogeneous fourth-order PDE driven by the leading-order axial flow solution. The fourth-order terms in this PDE form a biharmonic operator, and, to that end, the problem is similar to the plate stress problem considered by Liew and Wang [13], where a Rayleigh–Ritz method was formulated via an energy functional. However, our PDE governing Φ has additional lower-order terms, and there is no obvious equivalent of the energy functional. Nonetheless, we find that there does exist a relatively straightforward functional which is minimized by the stream function Φ. A Rayleigh–Ritz method for approximating the stream function then follows naturally, given an appropriate basis satisfying the boundary conditions. Since the PDEs for the higher-order u and Φ corrections differ only with respect to the inhomogeneous part, which depends on components that are already known, it is straightforward to use the method to approximate these terms as well. Furthermore, this can be adapted into an iterative method to obtain the complete flow solution.

Section 3.2 describes our specific implementation for ducts in which polynomials can be used to describe the shape of the top and bottom walls of the duct. These duct shapes are interesting to consider for two main reasons. The first is that modifications of the top and bottom wall shape are the most straightforward changes to make in the context of the typical manufacturing processes used to produce microfluidic devices. The second is that, with an appropriate basis, the integrals that need to be estimated can be calculated directly with very high accuracy (essentially only affected by floating-point rounding errors). We also examine how the conditioning of the linear system grows with the size of the basis, an issue which has been overlooked by previous works and can seriously inhibit the accuracy of the method if not addressed appropriately.

Section 4.1 provides and discusses solutions for several examples, including an example having an asymmetric trapezoidal cross-section inspired by that used for the experiments by Warkiani et al. [18]. By examining the decay in magnitude of higher-order terms in the perturbation expansion, we are also able to estimate the flow conditions in which the given perturbation expansion of the flow can be reasonably expected to converge. In Section 4.2 it is shown how quickly the Rayleigh–Ritz solutions converge towards high-order finite-element solutions, as the maximum degree of the polynomials used in the construction of the basis increases. We choose this as a form of verification due to a lack of readily available approximations for nonstandard duct shapes (particularly in relation to the secondary flow), and because it allows for a global error analysis as opposed to comparing some select summary statistics. Lastly, in Section 4.3 we describe a modification to handle curved (circular) pipes, and show that the Rayleigh–Ritz solutions are consistent with other results from the literature.

https://doi.org/10.1017/S1446181118000287 Published online by Cambridge University Press

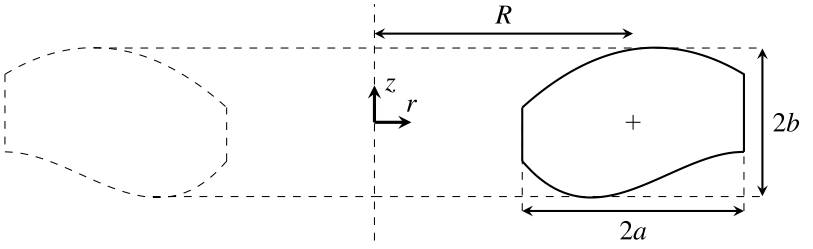

FIGURE 1. View of a rotationally symmetric duct in the plane of a fixed angle. The main axial flow is directed into the page. The cross-section after another π radians is also shown as a dashed outline on the left where the axial flow is directed out of the page (see text for details).

2. Governing equations of the flow

Consider a duct which is curved around the vertical z-axis, and exhibits rotational symmetry around this axis (that is, the cross-section does not vary with respect to the angle). With r as the radial coordinate with respect to the xy-plane, let the cross-section of the duct be described by a function $g(r, z)$ which is zero on the boundary and strictly positive in the interior. We require that $g(r, z)$ be three times differentiable over the cross-section. The centre of the cross-section is taken to be the centre of the smallest rectangle containing the cross-section. Let $2a$ and $2b$ denote the width and height of the bounding rectangle, respectively. The bend radius R is taken to be the distance of the centre from the z-axis. Without loss of generality, a duct can always be shifted vertically such that the centre of the cross-section is $(r, z) = (R, 0)$. To illustrate, a curved rectangular duct may be described by

$$g(r, z) = \{a^2 - (r - R)^2\}(b^2 - z^2).$$

The set-up for a nonrectangular example is depicted in Figure 1.

Suppose that the fluid flow through the duct is described by the Navier–Stokes equations. Consider a cylindrical coordinate system $\mathbf{x}(\theta, r, z) = r\cos\theta\hat{\mathbf{i}} + r\sin\theta\hat{\mathbf{j}} + z\hat{\mathbf{k}}$ with velocity vector $\mathbf{u} = (u, v, w)$, where the components denote the angular, lateral and vertical velocities, respectively. With the assumption that the fluid velocity is steady with respect to time, that is, $\partial\mathbf{u}/\partial t = \mathbf{0}$, and is independent of the angular coordinate, that is, $\partial\mathbf{u}/\partial\theta = 0$, the governing equations are

$$0 = \frac{\partial v}{\partial r} + \frac{\partial w}{\partial z} + \frac{v}{r}, \tag{2.1a}$$

$$\rho\left(v\frac{\partial u}{\partial r} + w\frac{\partial u}{\partial z} + \frac{2uv}{r}\right) = -\frac{1}{r^2}\frac{\partial p}{\partial \theta} + \mu\left(\frac{\partial^2 u}{\partial r^2} + \frac{\partial^2 u}{\partial z^2} + \frac{3}{r}\frac{\partial u}{\partial r}\right), \tag{2.1b}$$

$$\rho\left(v\frac{\partial v}{\partial r} + w\frac{\partial v}{\partial z} - ru^2\right) = -\frac{\partial p}{\partial r} + \mu\left(\frac{\partial^2 v}{\partial r^2} + \frac{\partial^2 v}{\partial z^2} + \frac{1}{r}\frac{\partial v}{\partial r} - \frac{v}{r^2}\right), \tag{2.1c}$$

$$\rho\left(v\frac{\partial w}{\partial r} + w\frac{\partial w}{\partial z}\right) = -\frac{\partial p}{\partial z} + \mu\left(\frac{\partial^2 w}{\partial r^2} + \frac{\partial^2 w}{\partial z^2} + \frac{1}{r}\frac{\partial w}{\partial r}\right). \tag{2.1d}$$

https://doi.org/10.1017/S1446181118000287 Published online by Cambridge University Press

We assume no-slip/penetration boundary conditions on the walls, that is, $\mathbf{u} = \mathbf{0}$ on the boundary described by $g(r, z) = 0$.

Equations (2.1) will be nondimensionalized similarly to Dean and Hurst [4] but with a different choice of scale for the secondary flow velocities. Let $\ell = \min\{a, b\}$ be a characteristic length scale for the duct cross-section (that is, analogous to taking the radius of a curved pipe as a characteristic length scale). Of particular interest are ducts that have height smaller than width, that is, $b \le a$ and thus $\ell = b$, since this is typical of the microfluidic ducts motivating this work. Introducing the new spatial variable s such that $r = R + s$ (and $dr = ds$), the duct cross-section can be described with respect to s, z by the function $\hat{g}(s, z) = g(R + s, z)$. The spatial variables s, z are nondimensionalized with respect to ℓ, that is, $z = \ell\hat{z}$ and $s = \ell\hat{s}$, whilst r is nondimensionalized with respect to R, that is, $r = R\hat{r}$. Defining $\epsilon = \ell/R$, notice that $\hat{r} = 1 + s/R = 1 + \epsilon\hat{s}$, and also $dr = R\,d\hat{r} = \ell\,d\hat{s}$. Now let U be a characteristic velocity for the axial velocity which we define to be the maximum of the (physical) axial velocity ru. With this, the axial velocity is nondimensionalized as $ru = U\hat{u}$, or equivalently $u = U\hat{u}/R\hat{r}$. The (duct) Reynolds number is defined as $\mathrm{Re} = \rho\ell U/\mu$. The secondary flow has a different scale than the axial flow, and so, taking V to be the characteristic velocity of the secondary flow, the corresponding dimensionless velocity components are $v = V\hat{v}$ and $w = V\hat{w}$. We make the specific choice $V = \epsilon\,\mathrm{Re}\,U$ (or equivalently $V = \rho\ell^2U^2/\mu R$), since this ensures that the term ru^2 in (2.1c) is an $O(1)$ driver of the secondary flow even when $\epsilon\,\mathrm{Re}^2$ is small.

It remains to consider the nondimensionalization of the pressure. From (2.1) it can be deduced that the pressure must have the form $p = C\theta + q(r, z)$, where C is constant. It is typical to choose $C = -GR$ such that G is the pressure gradient per unit length along the centre of the duct. Therefore, one has $\partial p/\partial\theta = -GR$, $\partial p/\partial r = \partial q/\partial r$ and $\partial p/\partial z = \partial q/\partial z$. The pressure gradient G may be nondimensionalized as $G = \mu U\hat{G}/\ell^2$ with the specific value of $\hat{G}$ fixed such that $\hat{u}$ has a maximum of 1 to be consistent with the chosen characteristic velocity U (and therefore the value of $\hat{G}$ will depend on the specific shape of the cross-section). On the other hand, the remaining pressure component q only features in the momentum equations for the secondary flow velocities and is, therefore, nondimensionalized as $q = \mu V\hat{q}/\ell$.

Putting all of this together, the equations (2.1) in dimensionless form are

$$0 = \frac{1}{\hat{r}}\left(\frac{\partial(\hat{r}\hat{v})}{\partial\hat{s}} + \frac{\partial(\hat{r}\hat{w})}{\partial\hat{z}}\right), \tag{2.2a}$$

$$K\left(\hat{r}\hat{v}\frac{\partial\hat{u}}{\partial\hat{s}} + \hat{r}\hat{w}\frac{\partial\hat{u}}{\partial\hat{z}} + \epsilon\hat{u}\hat{v}\right) = \hat{G} + \hat{r}\frac{\partial^2\hat{u}}{\partial\hat{s}^2} + \hat{r}\frac{\partial^2\hat{u}}{\partial\hat{z}^2} + \epsilon\frac{\partial\hat{u}}{\partial\hat{s}} - \epsilon^2\frac{\hat{u}}{\hat{r}}, \tag{2.2b}$$

$$K\left(\hat{v}\frac{\partial\hat{v}}{\partial s} + \hat{w}\frac{\partial\hat{v}}{\partial\hat{z}}\right) - \frac{\hat{u}^2}{\hat{r}} = -\frac{\partial\hat{q}}{\partial\hat{s}} + \frac{\partial^2\hat{v}}{\partial\hat{s}^2} + \frac{\partial^2\hat{v}}{\partial\hat{z}^2} + \epsilon\frac{1}{\hat{r}}\frac{\partial\hat{v}}{\partial\hat{s}} - \epsilon^2\frac{\hat{v}}{\hat{r}^2}, \tag{2.2c}$$

$$K\left(\hat{v}\frac{\partial\hat{w}}{\partial\hat{s}} + \hat{w}\frac{\partial\hat{w}}{\partial\hat{z}}\right) = -\frac{\partial\hat{q}}{\partial\hat{z}} + \frac{\partial^2\hat{w}}{\partial\hat{s}^2} + \frac{\partial^2\hat{w}}{\partial\hat{z}^2} + \epsilon\frac{1}{\hat{r}}\frac{\partial\hat{w}}{\partial\hat{s}}, \tag{2.2d}$$

where $K = \epsilon\,\mathrm{Re}^2$. Note that whilst some studies have taken the Dean number to be $2K$ (see, for example, [10]), others have taken (up to a constant factor)

https://doi.org/10.1017/S1446181118000287 Published online by Cambridge University Press

$\mathrm{Dn} = \sqrt{K} = \sqrt{\epsilon}\,\mathrm{Re}$ [7, 20]. We sometimes refer to K as the square of the Dean number to be consistent with the latter. Some studies also make use of the Dean approximation in which terms involving factors of $\epsilon = \ell/R$ are eliminated under the assumption $\epsilon \ll 1$ (noting it is always the case that $\epsilon \leq 1$). We do not take this approach, so that the resulting method can be applied in cases where ϵ is not so small. For ease of readability and convenience, the carets will be dropped in the remainder of the paper.

The continuity equation (2.2a) can be eliminated with the introduction of a (dimensionless) stream function Φ, for which $\partial\Phi/\partial s = rw$ and $\partial\Phi/\partial z = -rv$. The v and w components of the momentum equations (2.2c) and (2.2d) respectively can then be combined to eliminate the remaining pressure q (that is, by taking $-\partial/\partial z$ of equation (2.2c) and $\partial/\partial s$ of equation (2.2d), then adding the two). The resulting equations for u and Φ are

$$K\left(-\frac{\partial\Phi}{\partial z}\frac{\partial u}{\partial s} + \frac{\partial\Phi}{\partial s}\frac{\partial u}{\partial z} - \epsilon\frac{u}{r}\frac{\partial\Phi}{\partial z}\right) = G + r\Delta u + \epsilon\frac{\partial u}{\partial s} - \epsilon^2\frac{u}{r}, \tag{2.3a}$$

$$\begin{aligned} K\Bigg(&\epsilon\frac{2}{r^3}\frac{\partial^2\Phi}{\partial z^2}\frac{\partial\Phi}{\partial z} - \frac{1}{r^2}\frac{\partial\Phi}{\partial z}\frac{\partial\Delta\Phi}{\partial s} + \frac{1}{r^2}\frac{\partial\Phi}{\partial s}\frac{\partial\Delta\Phi}{\partial z} - \epsilon^2\frac{3}{r^4}\frac{\partial\Phi}{\partial z}\frac{\partial\Phi}{\partial s} \\ &+ \epsilon\frac{3}{r^3}\frac{\partial\Phi}{\partial z}\frac{\partial^2\Phi}{\partial s^2} - \epsilon\frac{1}{r^3}\frac{\partial\Phi}{\partial s}\frac{\partial^2\Phi}{\partial s\partial z}\Bigg) + \frac{2u}{r}\frac{\partial u}{\partial z} \\ &= \frac{1}{r}\Delta^2\Phi - \epsilon\frac{2}{r^2}\frac{\partial\Delta\Phi}{\partial s} + \epsilon^2\frac{3}{r^3}\frac{\partial^2\Phi}{\partial s^2} - \epsilon^3\frac{3}{r^4}\frac{\partial\Phi}{\partial s}, \end{aligned} \tag{2.3b}$$

where $\Delta = \partial^2/\partial s^2 + \partial^2/\partial z^2$. The boundary conditions for Φ are $\Phi = 0$ and $\partial\Phi/\partial\mathbf{n} = 0$ on the walls of the duct (where $\mathbf{n}$ denotes the unit normal vector of the boundary of the duct cross-section).

Now consider a perturbation expansion of u and Φ with respect to K, that is,

$$u = \sum_{i=0}^{\infty} K^i u_i\,, \quad \Phi = \sum_{i=0}^{\infty} K^i \Phi_i\,. \tag{2.4}$$

Note that whilst it is more common to see ϵ used as the perturbing parameter, we have found K to be useful since it incorporates the axial velocity scale. Substituting (2.4) into equations (2.3), and equating terms having the same power of K, we obtain

$$\sum_{j=0}^{i-1}\left(-\frac{\partial\Phi_j}{\partial z}\frac{\partial u_{i-1-j}}{\partial s} + \frac{\partial\Phi_j}{\partial s}\frac{\partial u_{i-1-j}}{\partial z} - \epsilon\frac{u_{i-1-j}}{r}\frac{\partial\Phi_j}{\partial z}\right) - G\delta_{i,0} = r\Delta u_i + \epsilon\frac{\partial u_i}{\partial s} - \epsilon^2\frac{u_i}{r}, \tag{2.5a}$$

$$\begin{aligned} \sum_{j=0}^{i-1}\Bigg(&\epsilon\frac{2}{r^3}\frac{\partial^2\Phi_j}{\partial z^2}\frac{\partial\Phi_{i-1-j}}{\partial z} - \frac{1}{r^2}\frac{\partial\Phi_j}{\partial z}\frac{\partial\Delta\Phi_{i-1-j}}{\partial s} + \frac{1}{r^2}\frac{\partial\Phi_j}{\partial s}\frac{\partial\Delta\Phi_{i-1-j}}{\partial z} - \epsilon^2\frac{3}{r^4}\frac{\partial\Phi_j}{\partial z}\frac{\partial\Phi_{i-1-j}}{\partial s} \\ &+ \epsilon\frac{3}{r^3}\frac{\partial\Phi_j}{\partial z}\frac{\partial^2\Phi_{i-1-j}}{\partial s^2} - \epsilon\frac{1}{r^3}\frac{\partial\Phi_j}{\partial s}\frac{\partial^2\Phi_{i-1-j}}{\partial s\partial z} + \sum_{j=0}^{i}\frac{2u_j}{r}\frac{\partial u_{i-j}}{\partial z}\Bigg) \\ &= \frac{1}{r}\Delta^2\Phi_i - \epsilon\frac{2}{r^2}\frac{\partial\Delta\Phi_i}{\partial s} + \epsilon^2\frac{3}{r^3}\frac{\partial^2\Phi_i}{\partial s^2} - \epsilon^3\frac{3}{r^4}\frac{\partial\Phi_i}{\partial s}, \end{aligned} \tag{2.5b}$$

https://doi.org/10.1017/S1446181118000287 Published online by Cambridge University Press

with $\delta_{i,0}$ the Kronecker delta. For each u_i we require only the u_j, Φ_j terms with $j < i$ to obtain a solution. To solve for Φ_i we additionally need u_i. For example, the equations for the leading-order terms u_0 and Φ_0 are

$$-G = r\Delta u_0 + \epsilon\frac{\partial u_0}{\partial s} - \epsilon^2\frac{u_0}{r}, \tag{2.6a}$$

$$\frac{2u_0}{r}\frac{\partial u_0}{\partial z} = \frac{1}{r}\Delta^2\Phi_0 - \epsilon\frac{2}{r^2}\frac{\partial\Delta\Phi_0}{\partial s} + \epsilon^2\frac{3}{r^3}\frac{\partial^2\Phi_0}{\partial s^2} - \epsilon^3\frac{3}{r^4}\frac{\partial\Phi_0}{\partial s}. \tag{2.6b}$$

Similarly, the equations for the $O(K)$ terms u_1 and Φ_1 are

$$\begin{aligned}
&-\frac{\partial\Phi_0}{\partial z}\frac{\partial u_0}{\partial s} + \frac{\partial\Phi_0}{\partial s}\frac{\partial u_0}{\partial z} - \epsilon\frac{u_0}{r}\frac{\partial\Phi_0}{\partial z} = r\Delta u_1 + \epsilon\frac{\partial u_1}{\partial s} - \epsilon^2\frac{u_1}{r},\\
&\epsilon\frac{2}{r^3}\frac{\partial^2\Phi_0}{\partial z^2}\frac{\partial\Phi_0}{\partial z} - \frac{1}{r^2}\frac{\partial\Phi_0}{\partial z}\frac{\partial\Delta\Phi_0}{\partial s} + \frac{1}{r^2}\frac{\partial\Phi_0}{\partial s}\frac{\partial\Delta\Phi_0}{\partial z} - \epsilon^2\frac{3}{r^4}\frac{\partial\Phi_0}{\partial z}\frac{\partial\Phi_0}{\partial s}\\
&\qquad + \epsilon\frac{3}{r^3}\frac{\partial\Phi_0}{\partial z}\frac{\partial^2\Phi_0}{\partial s^2} - \epsilon\frac{1}{r^3}\frac{\partial\Phi_0}{\partial s}\frac{\partial^2\Phi_0}{\partial s\partial z} + \frac{2u_0}{r}\frac{\partial u_1}{\partial z} + \frac{2u_1}{r}\frac{\partial u_0}{\partial z}\\
&\qquad = \frac{1}{r}\Delta^2\Phi_1 - \epsilon\frac{2}{r^2}\frac{\partial\Delta\Phi_1}{\partial s} + \epsilon^2\frac{3}{r^3}\frac{\partial^2\Phi_1}{\partial s^2} - \epsilon^3\frac{3}{r^4}\frac{\partial\Phi_1}{\partial s}.
\end{aligned}$$

In the general case, we use $f_i^{(u)}$ and $f_i^{(\Phi)}$ to denote the left-hand side of the equations (2.5a) and (2.5b), respectively, for brevity.

3. A Rayleigh–Ritz method

3.1. Derivation Let $i \in \mathbb{N}$ (taking $\mathbb{N} = \{0, 1, 2, \dots\}$) be fixed, and suppose that u_j, Φ_j are known for $j = 0, 1, \dots, i-1$. Since the equation (2.6a) governing u_0 is exactly the Stokes flow model considered by Wang [16], the same Rayleigh–Ritz method can be used and is straightforward to adapt to the general case. In particular, the u_i which is a solution to (2.5a) is also the extremum of

$$J_i^{(u)} = \iint_\Omega r\left(\frac{\partial u_i}{\partial s}\right)^2 + r\left(\frac{\partial u_i}{\partial z}\right)^2 + \epsilon^2\frac{u_i^2}{r} + 2f_i^{(u)}u_i\,dz\,ds, \tag{3.1}$$

where Ω denotes the duct cross-section. This is easily verified via the classical Euler–Lagrange equations obtained via the calculus of variations. From here one considers expressing u_i as

$$u_i(s,z) = \sum_{n=1}^{\infty} c_n\phi_n(s,z) \tag{3.2}$$

with ϕ_n being an appropriate set of basis functions satisfying the boundary condition $\phi_n = 0$ on the walls of the duct. A typical choice is taking $\{\phi_n\}_{n\in\mathbb{N}}$ as the set of monomials $\{1, s, z, s^2, sz, z^2, s^3, s^2z, sz^2, z^3, \dots\}$ multiplied by the function $g(s,z)$. Substituting (3.2) into (3.1), one then takes $\partial J_i^{(u)}/\partial c_m = 0$ to obtain a linear equation of the form

$$\sum_n A_{m,n}^{(u)}c_n = B_m^{(u)}, \tag{3.3}$$

https://doi.org/10.1017/S1446181118000287 Published online by Cambridge University Press

for each m (noting the sum on the right-hand side of equation (19) in [16] appears to be a typographical error), where

$$A^{(u)}_{m,n} = \iint_\Omega r\frac{\partial\phi_n}{\partial s}\frac{\partial\phi_m}{\partial s} + r\frac{\partial\phi_n}{\partial z}\frac{\partial\phi_m}{\partial z} + \epsilon^2\frac{\phi_n\phi_m}{r}\,dz\,ds, \tag{3.4a}$$

$$B^{(u)}_m = -\iint_\Omega \phi_m f^{(u)}_i\,dz\,ds. \tag{3.4b}$$

In practice, the basis is truncated so that the sums in equations (3.2) and (3.3) are finite. We refer to the degree of the approximation as the highest degree to which we truncate the sequence of monomials $\{1, s, z, s^2, sz, z^2, s^3, s^2z, sz^2, z^3, \dots\}$, used in the construction of the basis. For example, if D is the degree of the approximation then the truncated basis is

$$\{\phi_n\}_{n=1}^N = \{s^i z^j g(s,z) \mid i, j \in \mathbb{N} \text{ and } i + j \le D\}, \tag{3.5}$$

where $N = (D+1)(D+2)/2$ is the total number of terms. With each of the integrals in (3.4a) and (3.4b) evaluated for $n, m \in \{1, \dots, N\}$, an $N \times N$ linear system of equations is obtained from (3.3), and can be solved to find the coefficients c_n.

The u_0 solution is precisely an approximation to the Stokes flow solution (that is, the limit $\mathrm{Dn} \to 0$) which Wang [16] compared to a truncated Fourier–Bessel solution in the case of rectangular ducts, and found that both methods agreed within 0.1% with respect to the average flow velocity. Note that one could consider an alternative basis consisting of $g(s,z)$ multiplied by a sequence of polynomials which are orthogonal over the cross-section with respect to the integral (3.4a); however, as pointed out by Brown and Stone [2], the solution up to a given polynomial degree is (analytically) identical, and the effect is only to modify the numerical stability of the solution (the conditioning of $A^{(u)}$ in particular). The issue of stability and conditioning is explored in more detail in Section 3.2.

It is possible to make some optimizations and simplifications to the computation in some cases. Note that if the same basis $\{\phi_n\}$ used for each u_i, then the matrix $A^{(u)}$ needs only to be calculated/constructed once for a given duct , and only the vector $B^{(u)}$ needs to be updated for each i. As noted by Wang [16], if the duct cross-section happens to possess mirror symmetry with respect to z then u (and each u_i) is even with respect to z. Therefore, if one constructs g such that $g(s,-z) = g(s,z)$, then basis functions with odd j can be omitted in the expansion (3.2) of each u_i. Symmetry in the duct cross-section with respect to s cannot be exploited in the same way due to asymmetry induced in the flow with respect to s because of the duct being curved.

We now describe a similar Rayleigh–Ritz method for approximating the Φ_i terms by utilizing the following result.

Proposition 3.1. *The Φ_i which solves (2.5b) is a stationary point of*

$$J^{(\Phi)}_i = \iint_\Omega \frac{1}{r}\left(\frac{\partial^2\Phi_i}{\partial s^2} + \epsilon\frac{1}{r}\frac{\partial\Phi_i}{\partial s} + \frac{\partial^2\Phi_i}{\partial z^2}\right)^2 - \epsilon^2\frac{4}{r^3}\left(\frac{\partial\Phi_i}{\partial s}\right)^2 + \epsilon^2\frac{4}{r^3}\left(\frac{\partial\Phi_i}{\partial z}\right)^2 - 2f^{(\Phi)}_i\Phi_i\,dz\,ds. \tag{3.6}$$

https://doi.org/10.1017/S1446181118000287 Published online by Cambridge University Press

Proof. This is straightforward to verify via the Euler–Lagrange equations, that is, letting $\mathcal{L}$ denote the integrand of (3.6),

$$-\frac{\partial \mathcal{L}}{\partial \Phi_i} = -\frac{\partial}{\partial s}\frac{\partial \mathcal{L}}{\partial \Phi_{i,s}} - \frac{\partial}{\partial z}\frac{\partial \mathcal{L}}{\partial \Phi_{i,z}} + \frac{\partial^2}{\partial s^2}\frac{\partial \mathcal{L}}{\partial \Phi_{i,ss}} + \frac{\partial^2}{\partial s \partial z}\frac{\partial \mathcal{L}}{\partial \Phi_{i,sz}} + \frac{\partial^2}{\partial z^2}\frac{\partial \mathcal{L}}{\partial \Phi_{i,zz}},$$

with $\Phi_{i,s} = \partial \Phi_i/\partial s$, $\Phi_{i,z} = \partial \Phi_i/\partial z$ etc., is precisely equation (2.5b) up to a constant factor of 2. □

Similar to the u_i, we now consider an expansion of Φ_i of the form

$$\Phi_i(r, z) = \sum_{n=1}^{\infty} d_n \psi_n(r, z), \tag{3.7}$$

where ψ_n is an appropriate set of basis functions satisfying both the Dirichlet and Neumann boundary conditions. One such choice is to take the ψ_n as the set of monomials multiplied by $g(s, z)^2$. Note that by squaring g we ensure both $\psi_n = 0$ and $\partial \psi_n/\partial \mathbf{n} = 0$ are satisfied on the boundaries. Substituting (3.7) into (3.6) for each m, one then takes $\partial J_i^{(\Phi)}/\partial d_m = 0$ to form the linear equation

$$\sum_n A_{m,n}^{(\Phi)} d_n = B_m^{(\Phi)}, \tag{3.8}$$

where

$$A_{m,n}^{(\Phi)} = \iint_\Omega \frac{1}{r}\left(\frac{\partial^2 \psi_n}{\partial s^2} + \epsilon \frac{1}{r}\frac{\partial \psi_n}{\partial s} + \frac{\partial^2 \psi_n}{\partial z^2}\right)\left(\frac{\partial^2 \psi_m}{\partial s^2} + \epsilon \frac{1}{r}\frac{\partial \psi_m}{\partial s} + \frac{\partial^2 \psi_m}{\partial z^2}\right) - \epsilon^2 \frac{4}{r^3}\frac{\partial \psi_n}{\partial s}\frac{\partial \psi_m}{\partial s} + \epsilon^2 \frac{4}{r^3}\frac{\partial \psi_n}{\partial z}\frac{\partial \psi_m}{\partial z}\, dz\, ds, \tag{3.9a}$$

$$B_m^{(\Phi)} = \iint_\Omega \psi_m f_i^{(\Phi)}\, dz\, ds. \tag{3.9b}$$

As with the u_i, in practice, the basis (3.7) is truncated. We again refer to the degree of the approximation as the maximum degree of the polynomials used in the construction of the basis; in particular, if D is again the degree of the approximation, the truncated basis for Φ_i is

$$\{\psi_n\}_{n=1}^N = \{s^i z^j g(s, z)^2 \mid i, j \in \mathbb{N} \text{ and } i + j \le D\}, \tag{3.10}$$

where $N = (D + 1)(D + 2)/2$. Each of the integrals in (3.9a) and (3.9b) can then be estimated numerically for $n, m \in \{1, \ldots, N\}$ to form a linear $N \times N$ system of equations from (3.8), which can be solved to find the coefficients d_n. Note that the degree of the Φ_i approximation need not be the same as that of the u_i approximation; however, for convenience we have chosen to use the same degree for the results in Section 4, and therefore, use the same D and N here.

As with the case of the u_i, if the same basis is used for each Φ_i then the matrix $A^{(\Phi)}$ need only be computed/constructed once and only $B^{(\Phi)}$ needs to be updated for each subsequent i. Furthermore, if the duct cross-section possesses mirror symmetry with

https://doi.org/10.1017/S1446181118000287 Published online by Cambridge University Press

respect to z then Φ (and each Φ_i) is an odd function with respect to z and thus, given $g(s,z)$ which is even with respect to z, all basis functions with even j may be dropped from (3.10).

Note that, given these Rayleigh–Ritz methods for the u_i and Φ_i, we can also use them in an iterative scheme for directly estimating the complete u, Φ solutions by iterating on equations (2.3) with the inertial/quadratic terms on the left-hand side estimated by the preceding iterations. That is, letting $u^0, \Phi^0 = 0$, then for $k = 1, 2, \ldots$ until sufficiently converged one solves

$$K\Big(-\frac{\partial\Phi^{k-1}}{\partial z}\frac{\partial u^{k-1}}{\partial r} + \frac{\partial\Phi^{k-1}}{\partial r}\frac{\partial u^{k-1}}{\partial z} - \epsilon\frac{u^{k-1}}{r}\frac{\partial\Phi^{k-1}}{\partial z}\Big) = G + r\Delta u^k + \epsilon\frac{\partial u^k}{\partial r} - \epsilon^2\frac{u^k}{r},$$

$$\begin{aligned} K\Big(&\epsilon\frac{2}{r^3}\frac{\partial^2\Phi^{k-1}}{\partial z^2}\frac{\partial\Phi^{k-1}}{\partial z} - \frac{1}{r^2}\frac{\partial\Phi^{k-1}}{\partial z}\frac{\partial\Delta\Phi^{k-1}}{\partial r} + \frac{1}{r^2}\frac{\partial\Phi^{k-1}}{\partial r}\frac{\partial\Delta\Phi^{k-1}}{\partial z} \\ &- \epsilon^2\frac{3}{r^4}\frac{\partial\Phi^{k-1}}{\partial z}\frac{\partial\Phi^{k-1}}{\partial r} + \epsilon\frac{3}{r^3}\frac{\partial\Phi^{k-1}}{\partial z}\frac{\partial^2\Phi^{k-1}}{\partial r^2} - \epsilon\frac{1}{r^3}\frac{\partial\Phi^{k-1}}{\partial r}\frac{\partial^2\Phi^{k-1}}{\partial r\partial z}\Big) + \frac{2u^k}{r}\frac{\partial u^k}{\partial z} \\ &= \frac{1}{r}\Delta^2\Phi^k - \epsilon\frac{2}{r^2}\frac{\partial\Delta\Phi^k}{\partial r} + \epsilon^2\frac{3}{r^3}\frac{\partial^2\Phi^k}{\partial r^2} - \epsilon^3\frac{3}{r^4}\frac{\partial\Phi^k}{\partial r}. \end{aligned}$$

This would be expected to converge whenever $K = \mathrm{Dn}^2$ is small enough such that the perturbation series (2.4) converges for a given duct shape.

3.2. Implementation Whilst the method described above is quite general, we describe here an implementation for computing the solution for a specific family of duct shapes. Consider curved ducts whose cross-section has a boundary easily described by height functions $h_{\mathrm{bot}}(s)$ and $h_{\mathrm{top}}(s)$ which provide the z value of the bottom and top walls of the duct, respectively, for all $s \in [-a, a]$. It is additionally assumed that $h_{\mathrm{bot}}(s)$, and $h_{\mathrm{top}}(s)$ are polynomials and $h_{\mathrm{bot}}(s) < h_{\mathrm{top}}(s)$ for all $s \in (-a, a)$. If $h_{\mathrm{top}}(-a) \neq h_{\mathrm{bot}}(-a)$ and/or $h_{\mathrm{top}}(a) \neq h_{\mathrm{bot}}(a)$, then the duct is closed by the addition of appropriate side walls, that is, the domain is $\Omega = \{(s,z) \mid s \in [-a,a],\ z \in [h_{\mathrm{bot}}(s), h_{\mathrm{top}}(s)]\}$. This family of duct shapes is relevant in the context of microfluidics, since such modifications of the top and bottom wall are relatively straightforward with the processes often used in the manufacture of such devices (micro-milling, photolithography, stereolithography, etc.). Furthermore, we are able to explicitly define a general $g(s,z)$ for this family of duct shapes, and provide a modified basis in which the integrals that need to be computed in the construction of the linear system become simple to evaluate.

For the cross-sections described above one may take

$$g(s,z) = (a^2 - s^2)(z - h_{\mathrm{bot}}(s))(h_{\mathrm{top}}(s) - z).$$

Given $h_{\mathrm{top}}(s)$ and $h_{\mathrm{bot}}(s)$ as polynomials in s, then the integrands of (3.4b) and (3.9) become rational polynomials in s, z. However, the denominators in each case are simply powers of $r = 1 + \epsilon s$ and can be eliminated with a careful modification of the basis. In particular, upon taking the truncated basis for u_i and Φ_i to be

$$\{\phi_n\}_{n=1}^N = \{(s/a)^i (z/b)^j g(s,z)(1+\epsilon s) \mid i, j \in \mathbb{N} \text{ and } i + j \leq D\}, \tag{3.11a}$$

$$\{\psi_n\}_{n=1}^N = \{(s/a)^i (z/b)^j g(s,z)^2 (1+\epsilon s)^3 \mid i, j \in \mathbb{N} \text{ and } i + j \leq D\}, \tag{3.11b}$$

https://doi.org/10.1017/S1446181118000287 Published online by Cambridge University Press

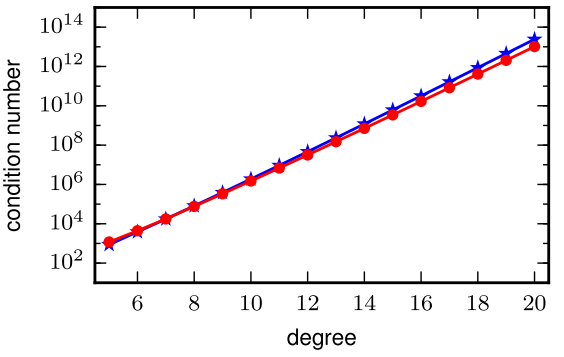

FIGURE 2. Condition number of $A^{(u)}$ (blue, star) and $A^{(\Phi)}$ (red, circle) versus the maximum degree of the polynomials used in the construction of the basis. The duct cross-section in this particular example is rectangular with $a = 2$, $b = 1$ and $R = 100$. Results are qualitatively similar for other duct cross-sections (colour available online).

respectively, then the integrands of (3.4b) and (3.9) become standard polynomials in s, z. These can be evaluated almost exactly (that is, up to floating-point rounding errors), since upon obtaining the indefinite integral with respect to z first, the two integration limits $h_{\text{bot}}(s), h_{\text{top}}(s)$ can be substituted to obtain a polynomial in s, which is then trivial to integrate over $[-a, a]$. Note also that in (3.11) the monomial factors $s^i z^j$ have been replaced with $(s/a)^i (z/b)^j$ in order to partially normalize with respect to the duct dimensions. Some examples of such ducts of this form and their corresponding solutions are provided in Section 4.1.

It is noteworthy that as one increases the degree D of the Rayleigh–Ritz approximation, the condition number of $A^{(u)}_{m,n}$ and $A^{(\Phi)}_{m,n}$ grows exponentially (see Figure 2). This means that even small rounding errors accumulated in the evaluation of the integrals in (3.4b) and (3.9) can have a large effect on the computed coefficients. There are several strategies one could take to alleviate the effects of high condition number, including but not limited to choosing a different basis, adding some form of regularization, or using multi-precision arithmetic. Whilst this is perhaps not the most attractive solution, given the additional computational cost associated with multi-precision arithmetic, it provides a benchmark against which other approaches can be measured, since it ensures the problem is solved accurately even when the condition number is large. Our implementation consists of a minimal polynomial class and linear algebra routines written in C++ which use the MPFR C library to provide multiple-precision arithmetic. Note that once the coefficients have been computed, the use of multiple-precision arithmetic is generally no longer necessary, that is, the coefficient vectors c, d can be rounded back to double-precision floating-point numbers (since the calculation of (3.2) and (3.7), given the bases (3.5) and (3.10), can be done in a stable manner). For the results reported in Section 4, the coefficients (computed in multi-precision) were rounded to double-precision floating-point numbers prior to the evaluation of u, Φ.

https://doi.org/10.1017/S1446181118000287 Published online by Cambridge University Press

The use of an alternative basis was considered. An ideal basis would be orthogonal with respect to the integrals that define $A^{(u)}$ and $A^{(\Phi)}$. However, such a basis would depend on the shape of the domain, making it difficult to implement in a general way. A simple modification of the basis that one might try, in general, is to use Chebyshev polynomials, since they are well known to be better behaved numerically than monomials in many applications. Specifically, the $(s/a)^i(z/b)^j$ factors in (3.11) could be replaced with $T_i(s/a)T_j(z/b)$, where $T_n(x)$ denotes the Chebyshev polynomial of degree n. Indeed, this choice of basis reduces the condition number by several orders of magnitude in the specific case of a rectangular duct. However, for nonrectangular ducts we found that using Chebyshev polynomials did not improve the conditioning, and for this reason, chose to use monomials to maintain the simplicity of exposition.

The addition of a simplified form of Tikhonov regularization in solving (3.3) and (3.8) in a least-squares sense was also considered. Specifically, we solved the modified linear systems

$$(A^{(u)\mathsf{T}}A^{(u)} + \alpha^2\mathbb{I})c = A^{(u)\mathsf{T}}B^{(u)}, \quad (A^{(\Phi)\mathsf{T}}A^{(\Phi)} + \beta^2\mathbb{I})d = A^{(\Phi)\mathsf{T}}B^{(\Phi)},$$

respectively, where α, β are regularization parameters and $\mathbb{I}$ is the identity matrix. In the case of a rectangular duct for degrees $10 < D \leq 20$, a choice of $\alpha = 1/10$ and $\beta = 1$ kept the conditioning of the new matrices below 2×10^6, whilst providing a solution that differed less than 0.1% from that obtained using multi-precision arithmetic (measured as a relative L_2 norm of the u_i, Φ_i constructed from both regularized and nonregularized c, d solutions, respectively). An advantage of using regularization is that the computations can be performed in double-precision floating-point arithmetic, but simultaneously there is a trade-off in the accuracy of the method. A more complete analysis of different types of regularization and their effect on the solution remains the subject of further investigation.

4. Results and discussion

4.1. Solutions for several examples Here we examine the flow solutions for several different duct shapes which are obtained using the implementation described in Section 3.2. Consider a rectangular, trapezoidal and bulging cross-section defined by the zero level set curves (restricted to $s \in [-2, 2]$) of

$$\begin{aligned} g_{\text{rect.}}(s, z) &= (4 - s^2)(1 - z^2), \\ g_{\text{bulg.}}(s, z) &= (4 - s^2)((1 - s^2/16)^2 - z^2), \\ g_{\text{trap.}}(s, z) &= (4 - s^2)(1 + z)(8/10 + s/10 - z), \end{aligned}$$

respectively. Note that the trapezoidal duct case is nonsymmetric with respect to s and z, thereby illustrating that the method works equally well in such cases. Whilst the cross-sections chosen here all have similar aspect ratio a/b, the method works just as well for other aspect ratios and similar results can be expected. Much of the flow behaviour discussed herein is generally well known in the context of a rectangular duct, and thereby provides qualitative validation of the Rayleigh–Ritz method.

https://doi.org/10.1017/S1446181118000287 Published online by Cambridge University Press

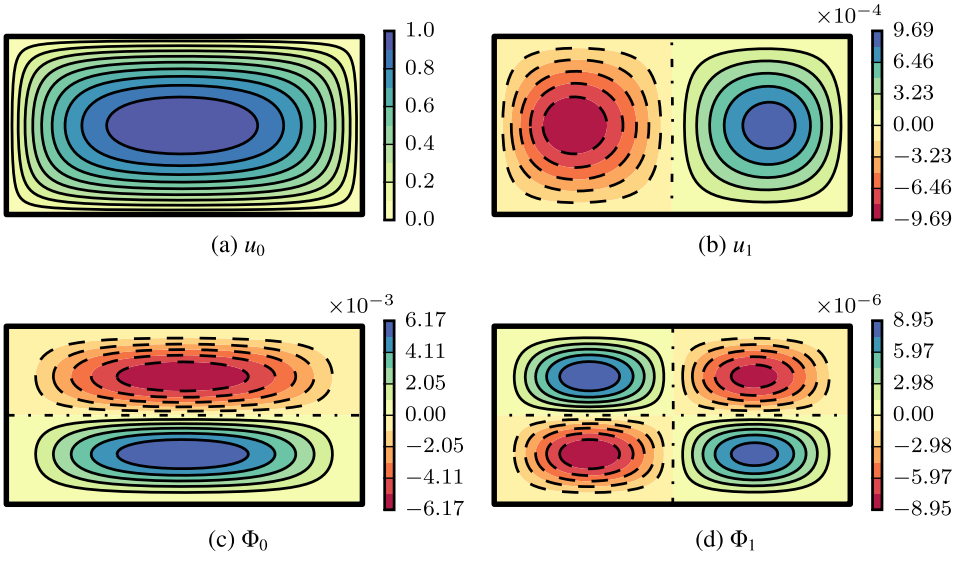

FIGURE 3. Degree-10 Rayleigh–Ritz approximations of the flow through a rectangular duct described by $g_{\text{rect.}}(s, z)$ with bend radius $R = 100$.

Considering first the case of a rectangular duct, in Figure 3 we plot solutions of u_i, Φ_i for $i = 1, 2$ when $R = 100$. Solid lines represent positive contours, dashed lines represent negative contours, and dash-dotted lines are the zero contour. The direction of secondary flow along the streamlines Φ_0, Φ_1 is clockwise around positive contours and anti-clockwise around negative contours. The leading-order axial flow solution u_0 is driven by the pressure gradient and is even with respect to z, owing to the vertical symmetry of the cross-section. Note, however, that u_0 is skewed horizontally, very slightly towards the inside wall (left edge) of the duct. This is explained by the Stokes solution favouring flow towards the inside wall as this provides a shorter path through the duct. The leading secondary flow solution Φ_0 is driven by the inertia of the leading-order axial flow. It is odd with respect to z, and shows the two circulations we expect to develop for flow in a curved duct. Like u_0, Φ_0 is also skewed very slightly towards the inside edge. The order-Dn^2 terms u_1, Φ_1 are driven by the inertia of the leading-order flow solution, and act to push the skew back towards the outside wall (right edge). It is seen from the small magnitude that a moderate Dn is necessary before this has appreciable impact on the flow. Like u_0, Φ_0, the u_1, Φ_1 solutions are even and odd with respect to z, respectively. Additionally, the vertical (dash-dotted) line for the zero contour is slightly left of centre because of the slight skewness in the leading-order flow components. Furthermore, the maximum magnitude of the solutions is slightly larger on the left-hand side of the zero-contour line. Note there are four circulation cells in Φ_1, which is indicative of the existence of four-vortex solutions when Dn is large (see, for example, [19, 20]), albeit that the perturbation expansion (2.4) used in

https://doi.org/10.1017/S1446181118000287 Published online by Cambridge University Press

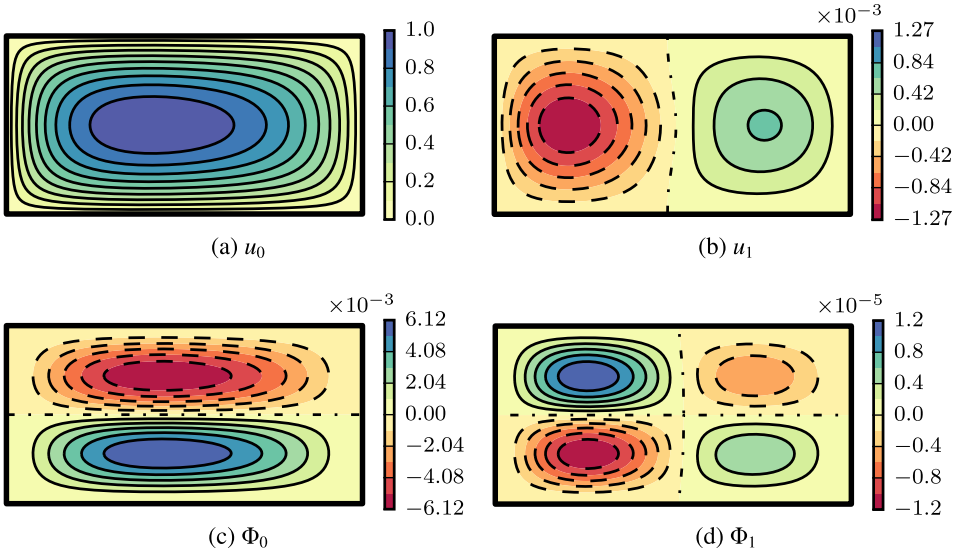

FIGURE 4. Degree-10 Rayleigh–Ritz approximations of the flow through a rectangular duct described by $g_{\text{rect.}}(s, z)$ with bend radius $R = 10$.

our method is unlikely to converge at such high Dean numbers. Additional terms u_i, Φ_i for $i > 1$ are also straightforward to compute but are not shown here since their effect is small for $\mathrm{Dn}^2 = O(1)$.

In Figure 4 we plot the solutions of u_i, Φ_i for $i = 1, 2$ again for the same rectangular duct, but with the smaller bend radius $R = 10$. The solutions are similar to those in Figure 3, except that the larger curvature of the duct exacerbates the skew in the solution towards the left (inside) wall of the duct. The difference in magnitude on the left- and right-hand sides of the order Dn^2 solutions is also more clearly evident. Note that one might expect the increased curvature to amplify the magnitude of the secondary flow, but observe that our nondimensionalization is such that the magnitude of Φ_0 has not changed significantly.

We now move on to look at solutions for the nonrectangular ducts. Figure 5 depicts the solutions for flow through the bulging cross-section shape with $R = 100$. Qualitatively, the flow behaviour is similar to the rectangular case with $R = 100$ but is "stretched" to fit the shape of the cross-section. Like the rectangular duct, the solutions for the u_i and Φ_i components are even and odd with respect to z, respectively, owing to the vertical symmetry of the cross-section. The solutions are again slightly skewed towards the inside wall of the duct, although to an even lesser extent than the rectangular case in Figure 3, because the bulging shape concentrates the axial flow more towards the centre. The effect of u_1 and Φ_1 for moderate Dn is again to effectively push the skew in u_0 and Φ_0, respectively, towards the outside wall.

Solutions for u_0, u_1, Φ_0, Φ_1 in the case of the asymmetric trapezoidal duct are shown

https://doi.org/10.1017/S1446181118000287 Published online by Cambridge University Press

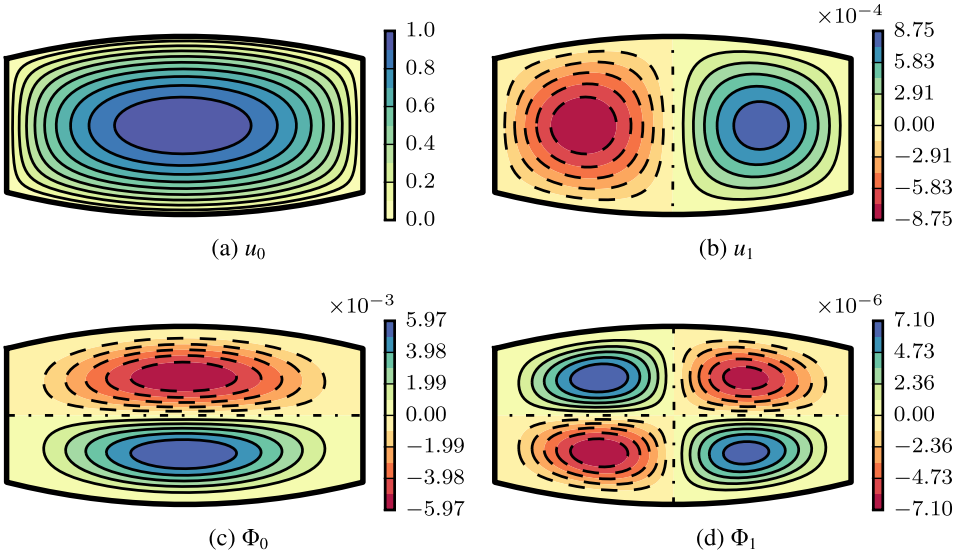

FIGURE 5. Degree-10 Rayleigh–Ritz approximations of the flow through a duct with a bulging cross-section described by $g_{\text{bulg.}}(s,z)$ having width $2a = 4$, height $2b = 2$ in the centre, and bend radius $R = 100$.

in Figure 6. Since this cross-section has neither symmetry with respect to z nor s, the solutions differ from the previous cases. The u and Φ components are no longer even and odd, respectively, with respect to z due to the loss of vertical symmetry. It may initially appear that Φ_0 is odd with respect to the zero-contour line, but on closer inspection it is evident that this is not the case. Since the duct is taller towards the outside edge, it can be seen that the leading-order axial flow u_0 favours the right-hand side to some extent, because the pressure gradient leads to faster flow where the surrounding area is greater. As a consequence, similar skew towards the outside wall is observed in each of Φ_0, u_1 and Φ_1. The Φ_0 component demonstrates two circulations that occur as a result of the curvature which one could again interpret as being "stretched" from the result for the rectangular duct to fit the trapezoidal shape. Note, however, that the circulation in the lower half is affected to a lesser extent than that in the upper half. The u_1, Φ_1 components may be viewed as pushing the skew in the flow further towards the outside edge for moderate Dn.

Given the ability to compute many u_i and Φ_i terms, we can examine the magnitude as a function of i, and thereby estimate the largest K (and Dn) for which the perturbation expansion (2.4) converges. In Figure 7 we plot $\|u_i\|_2$ (excluding odd i) and $\|\Phi_i\|_2$ (excluding even i) for the rectangular duct (with the L_2 norm taken over the cross-section). The cases of the bulging and trapezoidal shaped ducts decay similarly and are therefore not shown. The slope is approximately constant for $i \geq 1$, demonstrating a geometric rate of decay. Being somewhat conservative, the perturbation expansion

https://doi.org/10.1017/S1446181118000287 Published online by Cambridge University Press

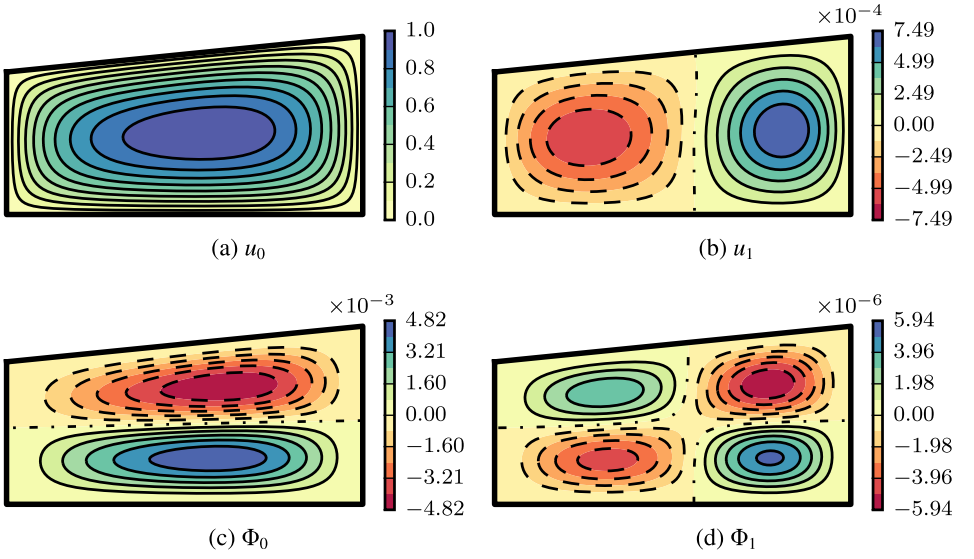

FIGURE 6. Degree-10 Rayleigh–Ritz approximations of the flow through a duct with an (asymmetric) trapezoidal cross-section described by $g_{\text{trap.}}(s, z)$ having width $2a = 4$, height $2b = 2$ in the centre, bend radius $R = 100$ and a slope on the top wall such that the height is 10% smaller at the left wall compared to the right wall.

(2.4) could be expected to converge for a given K, if there exists a $c \in [0, 1)$ such that

$$K\|u_{i+1}\|_2 \le c\|u_i\|_2 \quad \text{and} \quad K\|\Phi_{i+1}\|_2 \le c\|\Phi_i\|_2,$$

for all $i \ge 0$. Estimating the largest allowable K for which such a c exists from the data plotted in Figure 7 gives approximately $K = 212.3$, or equivalently, $\text{Dn} = 14.57$ (noting $\|u_3\|_2 \approx 212.3\|u_4\|_2$ gives the smallest estimate). However, for practical purposes we may wish to restrict K such that $c \le 1/2$ so that convergence is reasonably quick, in which case it would be reasonable to take the largest K to be approximately 100 (or equivalently, the largest Dn as approximately 10). To summarize, we conclude that our expansion of the flow through a curved duct is appropriate for applications with $\text{Dn} \le 10$, and furthermore, for $\text{Dn} = O(1)$, which is a common case for many microfluidic experiments, only one or two terms in the expansion may be needed.

4.2. Comparison with finite-element solutions In this section, we validate that our Rayleigh–Ritz method provides solutions which are globally consistent with those obtained via the finite-element method. In particular, the convergence (in an L_2 sense) of the Rayleigh–Ritz solutions with increasing degree towards a high-order finite-element solution is investigated. Recalling that $f_i^{(u)}$ is used to denote the left-hand sides of (2.5a), we obtain a standard weak formulation for the u_i, specifically

$$\int_\Omega -\nabla u_i \cdot \nabla v + \frac{\partial u_i}{\partial r}\frac{v}{r} - \frac{u_i v}{r}\, dA = \int_\Omega \frac{f_i^{(u)} v}{r}\, dA,$$

https://doi.org/10.1017/S1446181118000287 Published online by Cambridge University Press

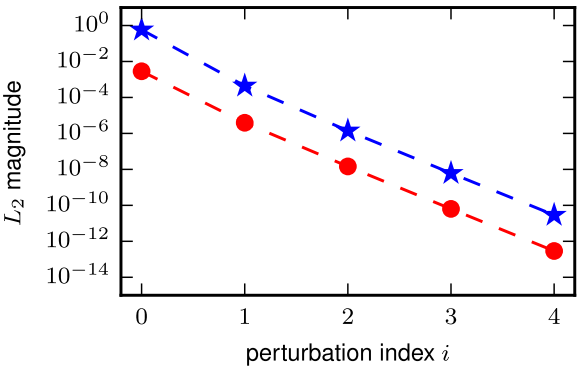

FIGURE 7. Plot of $\|u_i\|_2$ (blue $\star$) and $\|\Phi_i\|_2$ (red $\bullet$) versus the perturbation index i for a rectangular duct with $a = 2$, $b = 1$ and $R = 100$. Results are similar for other duct cross-sections (colour available online).

where v denotes a suitable test function. We implement this using FEniCS [1] with the domain Ω discretized as a triangular mesh (of approximately 40 000 cells) over which quadratic Lagrangian elements are used, and the Dirichlet boundary conditions are enforced explicitly at the linear algebraic level. The Φ_i are a little more complex to solve, being governed by the fourth-order PDE (2.5b). As both Dirichlet and Neumann boundary conditions must be enforced for the Φ_i, we apply an interior penalty implementation of the biharmonic $\Delta^2\Phi_i$ term (having multiplied (2.5b) by r), based on the discontinuous Galerkin method described by Georgoulis and Houston [9]. For the remaining terms in (2.5b) we simply multiply by the appropriate test function and integrate as per usual. Quartic Lagrangian elements are used as a basis for Φ_i over the same mesh used for the u_i. In order to compare solutions obtained from the two methods accurately, the Rayleigh–Ritz approximations are interpolated onto the same finite-element spaces used to compute the finite-element solutions. We then proceed to compute the L_2 norm of the difference between the two, and divide by the L_2 norm of the finite-element solution in order to obtain a relative error. Note that whilst it would be sufficient to use linear and cubic Lagrange elements for u_i and Φ_i, respectively, we choose to use one degree higher in order to improve the accuracy of the finite-element solutions and reduce the error which is introduced when interpolating the Rayleigh–Ritz approximations.

In Figure 8 we show the convergence of the Rayleigh–Ritz approximations u_0, u_1, Φ_0, Φ_1 to their corresponding finite-element solutions with respect to the polynomial degree of the basis. Observe that even with only terms up to degree 5, the relative error is of the order of 10^{-2} or smaller for each of the terms. This steadily decreases in each case as the degree of the basis increases, down towards a relative error of the order of 10^{-5} when the degree is 20 for u_0, Φ_0 and u_1. Note that Φ_1 seems to reach an asymptote at around 10^{-4}, because the difference in the finite-element and Rayleigh–Ritz approximations becomes dominated by the error of the finite-element solution. For the same reason, the improvement in relative error

https://doi.org/10.1017/S1446181118000287 Published online by Cambridge University Press

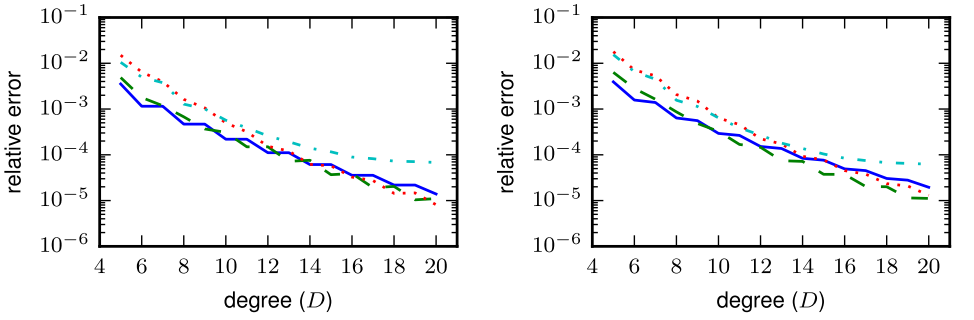

(a) Rectangular cross-section (b) Trapezoidal cross-section

FIGURE 8. Relative convergence of Rayleigh–Ritz approximations of u_0 (blue, solid), Φ_0 (green, dashed), u_1 (red, dotted) and Φ_1 (cyan, dash-dotted) to their corresponding finite-element solutions with respect to the polynomial degree for the two different duct cross-sections (a) rectangular, and (b) trapezoidal. In each case, $R = 100$ is used (colour available online).

for the other three components also begins to flatten out beyond approximations of degree 20. Observe that no improvement is made to the approximation quality of u_0 in the case of a rectangular duct when going from an even to odd degree, because the addition of polynomials which are odd with respect to z does not affect an even function. One might expect, then, that Φ_0 should not improve going from an odd to even degree given it is even, since Φ is odd. However, one does not see this because Φ_0 is driven by u_0^2, and thereby improves in accuracy because of the better approximation of u_0. For larger degrees when the improvement in u_0 is diminishing, one can begin to see only marginal improvement in Φ_0 going from odd to even degree. In the case of a trapezoidal duct, this behaviour does not occur since the vertical symmetry is lost, although some step-like behaviour can still be observed, because the addition of even-degree terms to u_0 is generally more beneficial than the addition of odd-degree terms since the asymmetry is not too extreme. Generally speaking, the convergence of the Rayleigh–Ritz approximation is quite steady, albeit with a slow diminishing of returns as the degree increases. It is worth pointing out that most of the error is, in fact, concentrated near the corners of the cross-section, and that over the majority of the domain the agreement is even better than what the relative L_2 error suggests.

4.3. Flow through curved (circular) pipes Given the wealth of literature on flow through curved circular pipes, it is natural to consider if the approach described herein produces similar results. In this section we compare results with two particular results from the literature. The first of these is by Yanase et al. [20] who considered the flow through a curved (circular) pipe, both with and without the Dean approximation (where one takes $\epsilon = 0$), by computing solutions via a spectral collocation method. A strength of their approach is that they are able to approximate solutions at quite high Dean numbers (much higher than is practical for microfluidics), which allowed them to study the existence and stability of multiple solutions at high Dean numbers. In

https://doi.org/10.1017/S1446181118000287 Published online by Cambridge University Press

comparison, our method is not well suited for such large Dean numbers, although we are able to compare results with the smaller of the Dn reported in [20]. They report a total flux through the cross-section and the axial velocity at the centre (unfortunately, no summary statistics of the secondary flow are provided). The second is the work of Robertson and Muller [15] who considered the flow of Oldroyd-B fluids through curved pipes. They derive the first few terms of the solution with respect to a perturbation expansion in a/R (a being the cross-section radius), with their results being applicable to Newtonian fluids by setting the Weissenberg number to zero.

Note that for a circular pipe the top and bottom walls are described by $h_{\text{top}}(s) = -h_{\text{bot}}(s) = \sqrt{a^2 - s^2}$, where a is the radius of the pipe. Since these are not polynomials in s, the implementation described in Section 3.2 requires some modification to be used in this case. Since the formulation in Section 3.1 is quite general, one need only implement a quadrature routine to accurately evaluate the integrals (3.4b) and (3.9) over the desired cross-section. For the specific case of a circular cross-section, one can go even further and reformulate the problem in toroidal coordinates via the change of variables $s = \eta\cos(\alpha)$ and $z = \eta\sin(\alpha)$. This leads to

$$
\begin{aligned}
J_i^{(u)} &= \int_0^{2\pi}\int_0^1 \left[r\left(\frac{\partial u_i}{\partial \eta}\right)^2 + \frac{r}{\eta^2}\left(\frac{\partial u_i}{\partial \alpha}\right)^2 + \epsilon^2\frac{u_i^2}{r} + 2f_i^{(u)}u_i \right]\eta\, d\eta\, d\alpha, \\
J_i^{(\Phi)} &= \int_0^{2\pi}\int_0^1 \left[\frac{1}{r}\left(\frac{\partial^2\Phi_i}{\partial\eta^2} + \frac{2r-1}{r\eta}\frac{\partial\Phi_i}{\partial\eta} + \frac{1}{\eta}^2\frac{\partial^2\Phi_i}{\partial\alpha^2} - \frac{\epsilon\sin(\alpha)}{\eta r}\frac{\partial\Phi_i}{\partial\alpha}\right)^2 \right. \\
&\quad - \frac{4\epsilon^2\cos(2\alpha)}{r^3}\left(\frac{\partial\Phi_i}{\partial\eta}\right)^2 \\
&\quad \left. + \frac{4\epsilon^2\cos(2\alpha)}{\eta^2 r^3}\left(\frac{\partial\Phi_i}{\partial\alpha}\right)^2 + \frac{8\epsilon^2\sin(2\alpha)}{\eta r^3}\frac{\partial\Phi_i}{\partial\eta}\frac{\partial\Phi_i}{\partial\alpha} - 2f_i^{(\Phi)}\Phi_i \right]\eta\, d\eta\, d\alpha,
\end{aligned}
$$

where $r = 1 + \epsilon\eta\cos(\alpha)$. With the bases for u_i, Φ_i similarly transformed, a toroidal implementation of the method is straightforward to obtain. Taking $g(\eta, \alpha) = 1 - \eta^2$ provides solutions for a circular cross-section.

Using the Dean approximation, Yanase et al. [20] report a total flux of 36.84 and an axial velocity at centre of 22.45 for a Dean number of 96 (which is equivalent to Dn = $\sqrt{288}$ in our dimensionless scaling). We too can approximate solutions using the Dean approximation by simply setting $\epsilon = 0$, and obtain a total flux and centre velocity which is in perfect agreement. Figure 9 shows the Rayleigh–Ritz solution for the circular cross-section.

Our solutions are also in good agreement with the perturbation solution provided by Robertson and Muller [15]. Noting their comment that "the perturbation results are suspect much beyond a Reynolds number of 25.0", we have chosen to compare for Re = 25. Letting $u_{\text{RM}}, \Phi_{\text{RM}}$ denote the perturbation solution of Robertson and Muller (up to and including the terms of order $(a/R)^2$), respectively, we compute the relative difference via

$$
\|u - u_{\text{RM}}\|_2/\|u\|_2, \quad \|\Phi - \Phi_{\text{RM}}\|_2/|\Phi\|_2,
$$

https://doi.org/10.1017/S1446181118000287 Published online by Cambridge University Press

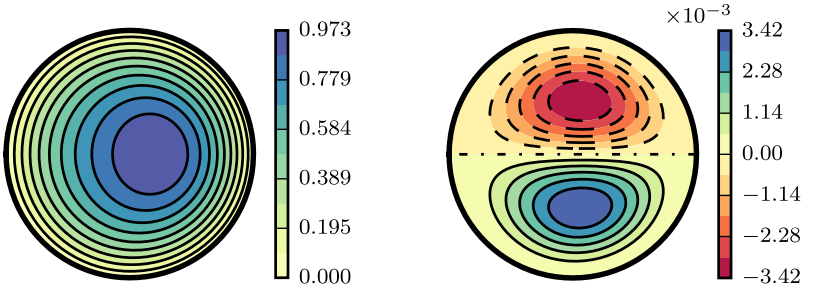

(a) u (b) Φ

FIGURE 9. Degree-15 Rayleigh–Ritz approximations of the flow through a curved duct with circular cross-section for $\mathrm{Dn} = \sqrt{288}$ and $G = 4$, using the Dean approximation.

where the norm $\|\cdot\|_2$ denotes the usual L_2 norm over the circular cross-section. Taking $a/R = 0.01$ such that $\mathrm{Dn} = 2.5$ and using a basis of degree 10, we obtain a relative difference of 6.35×10^{-7} and 1.84×10^{-4} for u and Φ, respectively.

5. Conclusions

We have extended a Rayleigh–Ritz method for approximating the axial flow through a curved duct [16] to the approximation of the secondary flow which develops within the cross-section. Additionally, we have demonstrated that it can be iterated to compute higher-order contributions with respect to the perturbation parameter Dn^2 such that a complete Navier–Stokes solution can be approximated, provided the Dean number is sufficiently small. We have developed an implementation specifically for duct shapes with top and bottom walls described by a polynomial, and have validated the method through the examination of several examples. A comparison with finite-element solutions demonstrates that our method converges reasonably quickly. Comparison with perturbation solutions in the case of a circular cross-section further validates the method.

Wang [16] previously argued that the Rayleigh–Ritz method is advantageous in that there is no need to discretize the domain. With the wide availability of meshing software for finite-element computations it is arguable that this is not such an advantage. However, a notable feature of the Rayleigh–Ritz solution is that once the coefficients have been computed they can be stored very cheaply and it is then straightforward and efficient to reconstruct the solution from the coefficients. This, in addition to the global nature of the solution, makes it particularly advantageous in the context of sampling it within larger and more complex computations, for instance the estimation of inertial lift forces in microfluidic devices briefly described in Section 1. Such cases are not so straightforward with piecewise approximations (including finite-element solutions), and will generally introduce additional approximation/sampling errors when meshes do not align perfectly.

https://doi.org/10.1017/S1446181118000287 Published online by Cambridge University Press

Previous studies of flow through curved rectangular and circular pipes have examined the existence and stability of multiple solutions at large Dean numbers. A potential extension of this work may be to modify the method so that it converges for similarly large Dn. Whilst such flow conditions are not of practical use in the context of microfluidics, it would allow one to study how perturbations to the shape of the cross-section may influence the existence and stability of multiple solutions. The issue of conditioning was briefly explored here, and could be investigated in more detail. Another potential extension is the implementation of Navier slip boundary conditions, thereby extending what has been done for the Stokes approximation of the axial flow by Wang [17].

Acknowledgement

This research was supported by Australian Research Council's Discovery Projects funding scheme (project number DP160102021).

References

[1] M. S. Alnæs, J. Blechta, J. Hake, A. Johansson, B. Kehlet, A. Logg, C. Richardson, J. Ring, M. E. Rognes and G. N. Wells, "The FEniCS project version 1.5", *Arch. Numer. Softw.* **3** (2015) 9–23; doi:10.11588/ans.2015.100.20553.

[2] R. E. Brown and M. A. Stone, "On the use of polynomial series with the Rayleigh–Ritz method", *Compos. Struct.* **39** (1997) 191–196; doi:10.1016/S0263-8223(97)00113-X.

[3] W. R. Dean XVI, "Note on the motion of fluid in a curved pipe", *Lond. Edinb. Dublin Philos. Mag. J. Sci.* **4** (1927) 208–223; doi:10.1080/14786440708564324.

[4] W. R. Dean and J. M. Hurst, "Note on the motion of fluid in a curved pipe", *Mathematika* **6** (1959) 77–85; doi:10.1112/S0025579300001947.

[5] D. Di Carlo, "Inertial microfluidics", *Lab Chip* **9** (2009) 3038–3046; doi:10.1039/B912547G.

[6] Y. Fan, R. I. Tanner and N. Phan-Thien, "Fully developed viscous and viscoelastic flows in curved pipes", *J. Fluid Mech.* **440** (2001) 327–357; doi:10.1017/S0022112001004785.

[7] G. P. Galdi and A. M. Robertson, "On flow of a Navier–Stokes fluid in curved pipes. Part I. Steady flow", *Appl. Math. Lett.* **18** (2005) 1116–1124; doi:10.1016/j.aml.2004.11.004.

[8] T. M. Geislinger and T. Franke, "Hydrodynamic lift of vesicles and red blood cells in flow – From Fåhræus and Lindqvist to microfluidic cell sorting", *Adv. Colloid Interface. Sci.* **208** (2014) 161–176; doi:10.1016/j.cis.2014.03.002.

[9] E. H. Georgoulis and P. Houston, "Discontinuous Galerkin methods for the biharmonic problem", *IMA J. Numer. Anal.* **29** (2009) 573–594; doi:10.1093/imanum/drn015.

[10] M. Germano, "The Dean equations extended to a helical pipe flow", *J. Fluid Mech.* **203** (1989) 289–305; doi:10.1017/S0022112089001473.

[11] B. Harding and Y. M. Stokes, "Fluid flow in a spiral microfluidic duct", *Phys. Fluids* **30** (2018) 042007; doi:10.1063/1.5026334.

[12] K. Hood, S. Lee and M. Roper, "Inertial migration of a rigid sphere in three-dimensional Poiseuille flow", *J. Fluid Mech.* **765** (2015) 452–479; doi:10.1017/jfm.2014.739.

[13] K. M. Liew and C. M. Wang, "pb-2 Rayleigh–Ritz method for general plate analysis", *Eng. Struct.* **15** (1993) 55–60; doi:10.1016/0141-0296(93)90017-X.

[14] J. M. Martel and M. Toner, "Particle focusing in curved microfluidic channels", *Sci. Rep.* **3** (2013) 3340; doi:10.1038/srep03340.

[15] A. M. Robertson and S. J. Muller, "Flow of Oldroyd-B fluids in curved pipes of circular and annular cross-section", *Int. J. Non-Lin. Mech.* **31** (1996) 1–20; doi:10.1016/0020-7462(95)00040-2.

[16] C. Y. Wang, "Stokes flow in a curved duct – A Ritz method", *Comput. Fluids* **53** (2012) 145–148; doi:10.1016/j.compfluid.2011.10.010.
[17] C. Y. Wang, "Ritz method for slip flow in curved micro-ducts and application to the elliptic duct", *Meccanica* **51** (2016) 1069–1076; doi:10.1007/s11012-015-0288-8.
[18] M. E. Warkiani, G. Guan, K. B. Luan, W. C. Lee, A. A. S. Bhagat, P. Kant Chaudhuri, D. S.-W. Tan, W. T. Lim, S. C. Lee, P. C. Y. Chen, C. T. Lim and J. Han, "Slanted spiral microfluidics for the ultra-fast, label-free isolation of circulating tumor cells", *Lab Chip* **14** (2014) 128–137; doi:10.1039/C3LC50617G.
[19] K. Yamamoto, X. Wu, T. Hyakutake and S. Yanase, "Taylor–dean flow through a curved duct of square cross section", *Fluid Dyn. Res.* **35** (2004) 67–86; doi:10.1016/j.fluiddyn.2004.04.003.
[20] S. Yanase, N. Goto and K. Yamamoto, "Dual solutions of the flow through a curved tube", *Fluid Dyn. Res.* **5** (1989) 191–201; doi:10.1016/0169-5983(89)90021-X.